and Fig. 5. Slight increase in prism compressive strength up to 100ºC is observed. Differences in compressive strength of concrete cured at 100ºC and 200ºC and control specimens kept only at the ambient temperature are negligible. On the contrary, the compressive strength significantly lowers after the recovering period. Similar effect of temperature elevation and recovering is observed for the impact strength. Evident losses in impact strength are found at any temperature elevation and recovering (Figure 5). Strength measures prove that structural degradation of concrete is markedly influenced by the temperature elevation. Rapid cooling of hot concrete surfaces exposed to 100ºC and 200ºC are for structural quality deterioration equally dangerous as the temperature elevations. This partial conclusion is confirmed by the cement paste study. The composition of the paste, which was based on that of the concrete, is given in Table 4. Compressive strength of concrete (Fig. 4) is always lower than that of the cement paste (Fig. 6) with the same mixture composition, temperature elevations, exposure times and curing conditions. It is believed that this is due to strength losses caused by interfacial transition zones between the cement paste and aggregate being regarded as the weakest of bulky concrete material. Compressive strength of the cement paste is decreases after recovery periods and shows similar trends of strength losses as observed in concrete specimens. Compressive strengths of the cement paste following the 28-day recovering period at 20°C / 60 % R.H. after exposure to 100°C and 200°C, are lower than those found after exposures to 100°C and 200°C. The shrinkage of the concrete was evident when cooled to the ambient 20°C; the explanation of this fact lies in crack propagation due to quick cooling and consequent strength losses that are not recoverable during following healing. Lasting and irreversible deterioration of the cement paste is found.

The cement paste or concrete once damaged by a higher temperature keeps its structural integrity disqualification even in the recovery period being regarded as "self-curing". The primary reason is rapid cooling of hot concrete to 20°C, resulting in crack propagation. The recovery at the ambient curing conditions after temperature attack does not contribute to the strength increase of a cement paste (or concrete). The drop in compressive strength of the cement paste after recovery periods is caused by the pore structure coarsening due to increases in volume of macropores (pore radius over 7 500 nm), pore median radius and total porosity (Table 5). The compressive strength dependence on parameters of the formed pore matrix is clearly reported in Table 6. The cement paste recovering after temperature exposure results higher portion of macropores, pore median radius and total porosity values. The larger air voids portion at lower compressive strength after recovering compared to the measured pore structure parameters and compressive strength of the cement paste kept only at 100°C and 200°C are observed.

Under freezing and thawing stabilized shrinkage at – 20 °C, negligible decrease in expansion at + 20 °C (Figure 7) and DME (Figure 8) of concrete relative to that in water is observed. Compressive strength is similar to that in water (Table 7). The pore structure of the concrete after freezing and thawing is changed when compared to that in water as follows: Increase in the volume and portion of macropores, micropore and pore median radius were found, and decrease in specific surface area of the pores, pore volume and total porosity was observed (Table 8). The pore structure is getting coarser but the compositions of the hydrate phase are similar (Table 9). The coarser pore structure in the concrete after freezing and thawing indicates the availability of water to develop hydraulic pressure but no evident deterioration of the specimens is found. This can be explained by the reduced amount of freezable water and also lower rate at which ice is forming due to dense pore structure with low permeability formed in the concrete rich in hydrate phase due to high cement content. Magnitude of deleterious hydraulic pressure is markedly eliminated by this way.

CONCLUSIONS

The following conclusions are applicable to the particular specimens and tests employed:

1. Pore structure coarsening at the end of recovery periods after 100°C and 200°C exposures results in significant concrete and cement paste strength decrease. Rapid cooling after temperature elevations evoke at least equal and irreversible pore structure deterioration of concrete and cement paste than that at 100 °C and 200 °C. This leads to strength losses that are not recoverable during healing at 20 °C. The primary reason is crack propagation evoked by rapid cooling. After recovery, cement matrix persistently deteriorates, and the impossibility to acquire its origin physical state before temperature attack is found.
2. Pore structure coarsening of the concrete after freezing and thawing is the result of water expansion due to freezing. The amount of the formed ice and magnitude of the hydraulic pressure are found at levels causing not evident crack propagation and structural degradation of concrete under given experimental conditions. It is thought that the primary reason is sufficiently low amount of freezable water available for ice forming in rich cementitious material concrete with the developed pore system.

REFERENCES

1. Noumowé, A. N., "Temperature Distribution and Mechanical Properties of High-Strength Silica-Fum Concrete at Temperatures up to 200 °C"; ACI Materials Journal, Vol. 100, 2003, pp. 326 – 330.

2. Mehta, P.K., "Concrete Technology and Crossroads – Problems and Opportunities, Paper published in symposium volume "V. Mohan Malhotra Symposium: Concrete Technology, Past, Present and Future", 1994, pp. 1 – 30. SP 144, Editor: P. Kumar Mehta.

Table 1. Physical Properties and Chemical Composition of Cement and Silica Fume

Chemical composition (%)	Cement	Silica fume	Physical properties	
			Cement	
Insoluble residue	1.50	–	Normal consistency (%)	30.6
SiO_2	19.84	94.16	Initial set (hour/min)	3/30
Al_2O_3	5.86	0.45	Final set (hour/min)	5/20
Fe_2O_3	2.84	0.98	Specific gravity ($kg.m^{-3}$)	3186
CaO	62.64	0.45	3-day strength* (MPa)	5.2/24.5
MgO	1.90	0.68	28-day strength (MPa)	10.5/47.6
SO_3	3.00	1.09	Silica fume	
Ign. loss (100°C)	0.47	0.54	Specific gravity ($kg.m^{-3}$)	2254
Ignition loss (100° – 1000°C)	1.91	1.61	Specific surface (BET) ($m^2.kg^{-1}$)	1425

*flexural/compressive

Table 2. Concrete Mixture Composition

Components	Per m^3
Portland cement of class 42.5	425 kg
Silica fume	32 kg
Aggregate: 0 / 4 mm	865 kg
Aggregate: 4 / 8 mm	393 kg
Aggregate: 8 / 16 mm	593 kg
Super plasticizer Melment	5.6 L
Water	136 L
Water / cement	0.32
Properties of fresh concrete	
Temperature	16 °C
Volume density	2440 $kg.m^{-3}$
Slump	60 mm
Air content	2 % vol.

Table 3. Compressive Strength of Concrete after 28-day Curing at 20°C/100 % R.H.

Size and shape of the specimens	Compressive strength, 28 days (MPa)
150 - mm cube	78.5
100 - mm cube	81.8
100x100x400 mm	63.1

Table 4. Cement Paste Composition in the Concrete (1000 L –1m³) Used for the Tests with the Cement Paste only (calculated on 1 liter)

Cement paste composition		
In tested concrete specimens	Constituents and ratios	Calculated for the tests with the cement paste only
425 kg	Cement	1.46 kg
32 kg	Silica fume	0.11 kg
5.6 L	Melment	0.0193 L
136.0 L	Water	0.47 L
13.28	Cement to silica fume	13.28
0.32	Water to cement ratio	0.32
0.0132	Melment to cement ratio	0.0132
0.041	Melment to water ratio	0.041

Table 5. Pore Structure Study of Cement Pastes

Curing regime used	Volume of macropores ($mm^3.g^{-1}$)	Portion of macropores (%)	Median of micropore radius (nm)	Median of pore radius (nm)	Total porosity (3.75 nm – 0.2 mm) (% vol.)
28 days basic	50.4	0	23.5	23.5	9.4
To 100°C	46.6	0	18.9	18.9	9.2
100°C + recovery	48.4	6.7	21.6	23.6	10.3
To 200 °C	55.9	4.4	23.1	23.7	11.2
200°C + recovery	41.7	5.2	31.8	32.6	11.9
20°C/60% R.H.	49.2	5.8	26.2	26.8	10.8

Table 6. Changes in Strength of Cement Paste related to Pore Structure Development at Ambient Curing and Temperature Elevations

Curing regime used	Portion of macropores (%)	Pore median radius (nm)	Total porosity (% vol.)	Compressive strength (MPa)
28 days basic	0	23.5	9.4	82.2
To 100°C	0	18.9	9.2	98.2
To 200°C	4.4	23.7	11.2	105.0
20°C/60% R.H.	5.8	26.8	10.8	115.3
To 100°C	0	18.9	9.2	98.2
100°C + recovery	6.7	23.6	10.3	91.8
To 200°C	4.4	23.7	11.2	105.0
200°C + recovery	5.2	32.6	11.9	97.7

Table 7. Prism Compressive Strength of the Concrete Kept in Water, after Freezing and Thawing and Kept in 20 °C / 60 % R.H. – air for Comparison

Curing	(abbreviated as)	Compressive strength (MPa)
Water, 20 °C	(W)	65.2
Freezing and thawing	(FT)	62.9
20 °C / 60 % R.H. – air	(D)	66.9

Table 8. Pore Structure Results of the Concrete at Various Curing Conditions

Parameter of the pore structure		Curing		
		W	FT	D
Specific surface area of pores	($m^2.g^{-1}$)	0.76	0.32	3.4
Volume of macropores	($mm^3.g^{-1}$)	3.1	4.2	2.0
Volume of micropores	($mm^3.g^{-1}$)	11.9	4.3	49.1
Total pore volume	($mm^3.g^{-1}$)	15.0	8.5	51.1
Micropore median radius	(nm)	13.6	274.9	24.8
Pore median radius	(nm)	14.9	664.7	25.3
Portion of macropores	(%)	2.0	49.2	4.0
Total porosity	(%)	3.4	1.9	9.7
Bulk density	($kg.m^{-3}$)	2 281	2 249	1 897

Table 9. Results of Thermal Analysis of the Concrete

Curing of the concrete specimens	Bound water content (%)	CaO bound in		Total CaO in $Ca(OH)_2$ and $CaCO_3$ (%)	Total ignition loss (%)
		$Ca(OH)_2$ (%)	$CaCO_3$ (%)		
W	2.45	0.86	2.06	2.91	8.25
FT	1.76	1.11	2.47	3.58	8.53

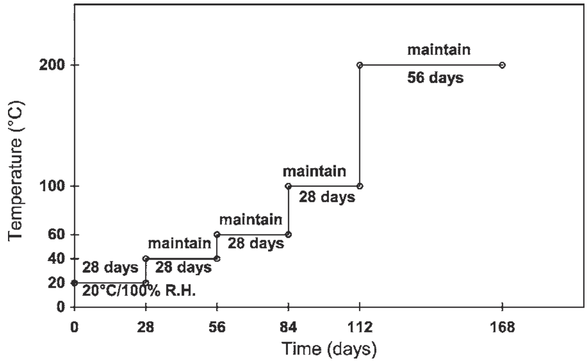

Fig. 1 — Temperature exposure conditions.

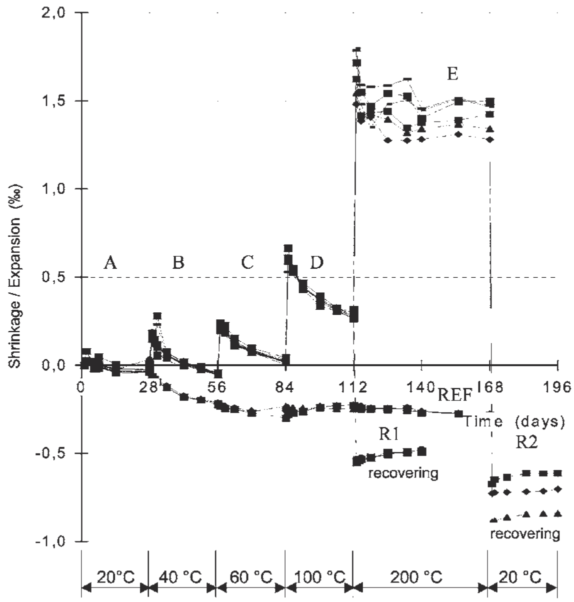

A: 28d 20°C / 100 % R.H.
B: 28d 20°C / 100 % R.H. + 28d 40°C
C: 28d 20°C / 100 % R.H. + 28d 40°C + 28d 60°C
D: 28d 20°C / 100 % R.H. + 28d 40°C + 28d 60°C + 28d 100°C
E: 28d 20°C / 100 % R.H. + 28d 40°C, 60°C, 100°C + 56d 200°C
R1: as D + 28d 20°C / 60 % R.H. (recovering)
R2: as E + 28d 20°C / 60 % R.H. (recovering)
REF: 28d 20°C / 100% R.H. + 140d 20°C / 60% R.H.

Fig. 2 — Length changes of concrete specimens.

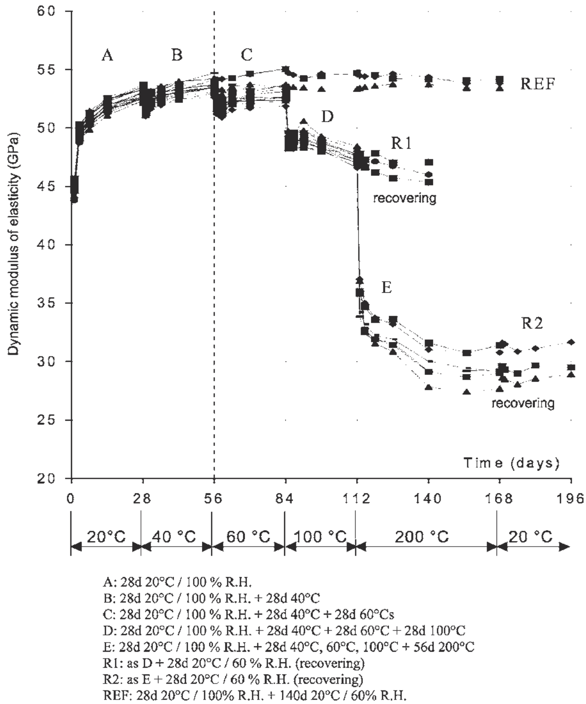

Fig. 3 — Dynamic modulus of elasticity at various temperature changes.

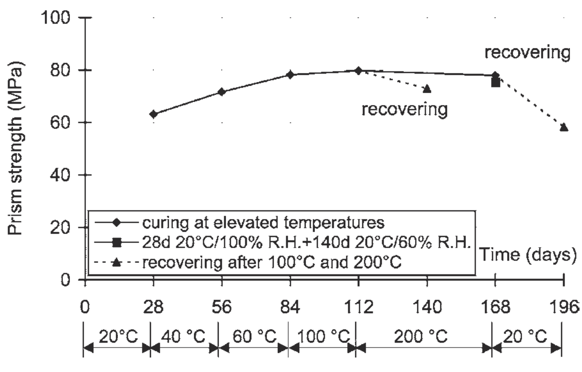

Fig. 4 — Prism compressive strength of concrete specimens.

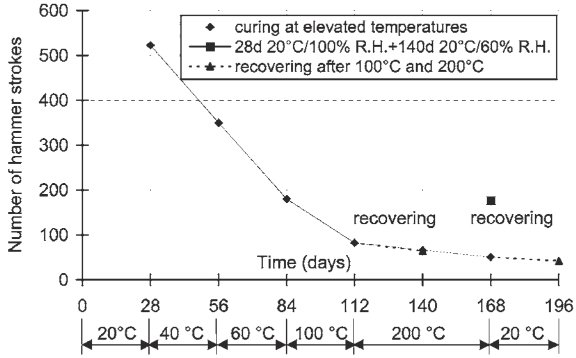

Fig. 5 — Impact strength of the specimens after temperature changes.

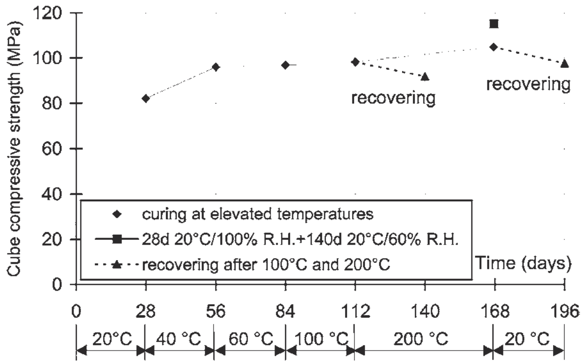

Fig. 6 — Cube compressive strength of cement paste prepared with the same composition as that in concrete.

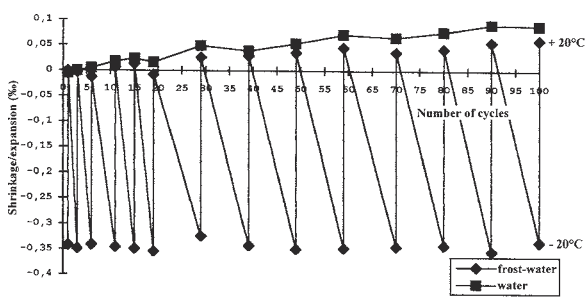

Fig. 7 — Shrinkage and expansion of the concrete at freezing and thawing.

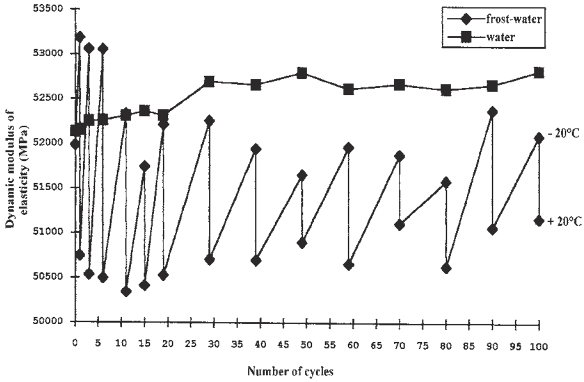

Fig. 8 — Changes in dynamic modulus of elasticity (DME) at freezing and thawing.

A Comparative Study on Mortar Containing Silica Fume and High Reactivity Metakaolin in Relation to Restrained Shrinkage Stress Development and Cracking

by A.B. Hossain, S. Islam, and B. Reid

Synopsis: Silica fume (SF) and high reactivity metakaolin (HRM) are two highly reactive pozzolans that offer excellent potential for use in high-performance concrete since concrete mixtures containing them demonstrate superior performance in terms of strength, and durability. High-performance concrete applications, such as pavements and bridge decks, are also required to demonstrate superior performance against early age shrinkage cracking. This paper describes a comparative study of the effects of SF and HRM on the early age stress development and cracking in restrained mortar mixtures due to shrinkage. The restrained ring test was used to assess early age residual stress development in mortar ring specimens. In addition, free shrinkage strains and splitting tensile strength measurements were performed to assess the cracking potential. It was found that the addition of SF and HRM increased the shrinkage level in the mixtures which resulted in increases in residual tensile stress development due to restraint. In addition, their addition in the mixtures increased the cracking potential and resulted in early cracking in the ring specimens.

Keywords: cracking potential; high reactivity metakaolin; mortar; shrinkage; silica fume